Proceedings of the 17th World Congress
The International Federation of Automatic Control
Seoul, Korea, July 6-11, 2008

Torque Multiplication and Singularity Avoidance in the Control of Electrostatic Torsional Micro-Mirrors ⋆

G. Zhu * **C.-G. Agudelo** * **L. Saydy** * **M. Packirisamy** **

* *Department of Electrical Engineering*
École Polytechnique de Montréal
C.P. 6079, Station Centre-Ville, Montréal, QC, Canada H3C 3A7
E-mail:
{guchuan.zhu,carlos-gustavo.agudelo,lahcen.saydy}@polymtl.ca
** *Department of Mechanical and Industrial Engineering*
Concordia University
1455 de Maisonneuve Blvd. West, Montréal, QC, Canada H3G 1M8
E-mail: pmuthu@alcor.concordia.ca

Abstract: The present work addresses the control of torsional micro-mirrors assisted by a constant bias voltage. It is shown that such a configuration will have an effect of torque multiplication and hence, it will reduce the dynamic range of actuation signal. A nonlinear controller using backstepping and barrier functions is developed, which can guarantee closed-loop stability in a restricted range covering a big portion of the physically allowable one, while eliminating the singularities due to uncontrollability and contact dynamics. In this study, the actuation voltage is taken as a state variable. This would further simplify the implementation of experimental systems. The development of the control algorithm has been demonstrated through a rectangular micro-mirror and the performance of the system is verified by numerical simulations. As a generic model is used in the design, the control algorithm developed can be applied to any device with the same structure regardless of the geometric shape.

1. INTRODUCTION

It is known that electrostatic actuation of torsional structures leads to a nonlinear dependency of the torque on the applied voltage across the device and to high nonlinear electrical dynamics due to the varying capacitance between the electrodes (see, e.g., Senturia [2002]). Due to this nonlinearity, the actuator moves hardly in the range of small deflection from its flat position (zero tilt angle) and becomes more sensitive to the span of the actuation signal as the tilt angle increases. This motivates the use of such a scheme in which a constant bias voltage is applied to shift the actuation signal to a steeper region on the voltage actuation curve (see Fig. 1), implementing the so-called torque multiplication (see, e.g., Hornbeck [1990], Pareek et al. [2005]) and helping to reduce the amplitude of the control signal. A schematic of such a configuration for one-degree of freedom (1DOF) torsional micro-mirrors is shown in Fig. 2. However, the bias voltage applied in such schemes causes a spring softening effect that makes the pull-in angle decrease, shortening the stable range of the micro-mirror when an open-loop control is used (see, e.g., Degani et al. [1998], Pareek et al. [2005]). This problem can be solved by using an appropriate closed-loop control which is capable of removing the pull-in.

Note that electrostatic actuation leads to systems which are not linearly controllable when the charge on the device is zero (see, e.g., Maithripala et al. [2005], Zhu et al. [2007], Agudelo et al. [2007a]). Therefore, any linearization-based control design will result in a singularity at this point. Applying a bias voltage would bring the operation point far from this singular point and therefore helps enhancing the controllability of the system.

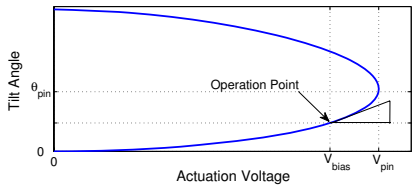

Fig. 1. Typical voltage actuation curve.

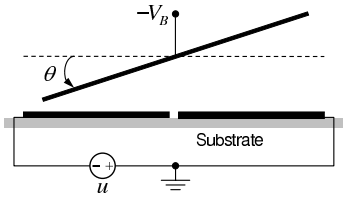

Fig. 2. Schematic cross section of torsional actuator with a bias configuration.

The movement of the micro-mirror is limited by physical constraints. It can be seen later on that when the movable plate hits the fixed one, the dynamics of the actuator exhibit a singularity. This might affect the stability of the system if the contact dynamics are not taken into account in controller design. As the behavior at the contact can be modelled by a switching system, the overall stability might be achieved by a proper design (see, e.g., Maithripala et al. [2005]). Another viable solution is to impose a hard constraint on the movement of the actuator. In the

⋆ This work was supported in part by NSERC (the Natural Sciences and Engineering Research Council of Canada) Discovery Grant.

literature, various techniques have been developed for control of constraint nonlinear systems, e.g., artificial potential field (Rimon and Koditschek [1992]), invariance control (Wolff and Buss [2005]), nonlinear reference governor (Bemporad [1998], Gilbert and Kolmanovsky [2001]), and Nonlinear Model Predictive Control (Bemporad [2003]). The method used in this work is the one based on backstepping with barrier functions introduced by Ngo et al. [2005]. This approach has the advantage of dealing with multiple state constraints using a recursive design procedure. This method has been applied to the control of a parallel-plate MEMS in the work of Tee et al. [2006] in order to saturate the movement of the device. In this work, we adapted this method to the control of torsional micro-mirrors. In addition to preventing the mirror from hitting the fixed electrode, we also consider the constraint on the actuation voltage, hence avoiding the aforementioned different singularities.

In this work we consider state feedback control. In practice, the angular velocity being not available for measurement, we can use state observers for closed-loop systems implementation (see, e.g., Zhu et al. [2006a], Agudelo et al. [2007a]).

The rest of the article is organized as follows. Section 2 addresses the modelling of generic 1DOF torsional micro-mirrors with bias voltage. Section 3 presents the control synthesis. Section 4 deals with the design details of the control of a rectangular micro-mirror. Section 5 reports on the simulations of the device being considered. Finally, Section 6 contains some concluding remarks.

2. MODELLING OF 1DOF MICRO-MIRRORS WITH BIAS VOLTAGE

First of all, we establish the dynamical model of 1DOF torsional micro-mirrors. When considered as a rigid body, the equation of motion of such devices is given by:

$$J\ddot{\theta} + b\dot{\theta} + k\theta = T_e, \tag{1}$$

where J is the mass moment of inertia of the movable electrode, b is the viscous damping coefficient, k is the the mechanical stiffness coefficient, and T_e is the applied electrical torque.

The capacitance due to a single electrode can be expressed as

$$C_a(\theta) = C_0\gamma(\theta), \tag{2}$$

where C_0 is the capacitance at the flat position and $\gamma(\theta)$ is a dimensionless scaling function satisfying $\gamma(0) = 1$. An advantage of expressing the capacitance of the device in the above generic form is that the control algorithm developed can be applied to any device of the same structure but with an arbitrary geometric shape.

The electrical torque produced by a single electrode can be obtained from differentiating the capacitance with respect to the angular deflection according to Senturia [2002]:

$$T_e = \frac{1}{2}V_a^2\frac{\partial C_a(\theta)}{\partial\theta} = \frac{1}{2}V_a^2 C_0\gamma'(\theta), \tag{3}$$

where V_a is the applied voltage across the device.

The dynamics of the electrical subsystem can be deduced from the equivalent circuit, including the amplifier and the actuator, as shown in Fig. 3, where R is output impedance of the voltage amplifier and C_p represents the parallel capacitor including the output capacitance of the voltage amplifier and the parasitics due to current leak. The control voltage V_s is composed of the bias V_B and the actuation signal u. When the charge on the

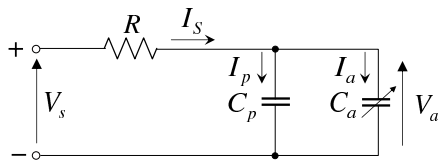

Fig. 3. Equivalent circuit.

device Q_a is taken as a state variable, the dynamical model of the electrical subsystem is given by Zhu et al. [2006b]:

$$\dot{Q}_a = \frac{C_a}{R(C_a + C_p)}\left(V_s - \frac{Q_a}{C_a^2}\left(C_a - RC_p\dot{C}_a\right)\right). \tag{4}$$

In the literature, it is common to consider the charge as a state variable. However, the implementation of on-chip charge measurement apparatus often results in a complex structure (see, e.g., Anderson et al. [2005]). In addition, the charge measurement is based essentially on the accumulation of the current across the actuator which is very weak for capacitive devices. For this reason, the charge measurement is prone to noise and low resolution, in addition to the off-set due to integration. Voltage measurement however is instantaneous and easy to implement, making the actuation voltage a better state variable candidate for control system design and implementation. By using the relationship $V_a = Q_a/C_a$ we can deduce from (4) that

$$\dot{V}_a = \frac{V_s - V_a}{RC_0\left(\rho + \gamma(\theta)\right)} - \frac{\dot{\theta}\gamma'(\theta)V_a}{\rho + \gamma(\theta)}, \tag{5}$$

where $\rho := C_p/C_0$, representing the influence of the parasitic capacitor.

Note that it is important to take into account the influence of the dynamics of the voltage amplifier. In particular, the output capacitance of the amplifier can be much higher than the one of the device in a large operating range. This has the effect of slowing down the actuation speed thus affecting the transition behavior as well as the stability of the system.

When the two electrodes are both charged, they will generate opposite electrical torques. In the sequel, we refer to the electrode that produces a counterclockwise (resp. clockwise) tilt when a voltage is applied as the positive (resp. negative) one. Letting C_{ep} and C_{en} be the capacitances due to the positive and negative electrodes, respectively, we then have

$$\begin{aligned} C_{ep}(\theta) =& C_0\gamma(\theta), \\ C_{en}(\theta) =& C_{ep}(-\theta) = C_0\gamma(-\theta). \end{aligned}$$

Denoting $\gamma_\theta = \gamma(\theta)$ and $\gamma_{-\theta} = \gamma(-\theta)$, the total electrical torque is given by:

$$T_e = \frac{1}{2}\left(C'_{ep}(\theta)V_{ap}^2 + C'_{en}(\theta)V_{an}^2\right) = \frac{C_0}{2}\left(\gamma'_\theta V_{ap}^2 + \gamma'_{-\theta}V_{an}^2\right) \tag{6}$$

where V_{ap} and V_{an} are the voltages across the positive and the negative electrodes, respectively.

Denoting by ω the angular velocity, we obtain from (1), (5), and (6) that

$$\dot{\theta} = \omega \tag{7a}$$

$$\dot{\omega} = \frac{1}{J}\left(-b\omega - k\theta + \frac{C_0}{2}\left(\gamma'_\theta V_{ap}^2 + \gamma'_{-\theta}V_{an}^2\right)\right) \tag{7b}$$

$$\dot{V}_{ap} = \frac{1}{RC_0\left(\rho + \gamma_\theta\right)}\left(V_{sp} - \left(1 + RC_0\omega\gamma'_\theta\right)V_{ap}\right) \tag{7c}$$

where V_{sp} is the control signal for the positive electrode. In the present scheme, the voltage across the negative electrode V_{an} is a constant.

Note that the contact of the movable and the fixed electrodes will result in shorting and rendering the electrical dynamics singular. A practical solution for preventing the device from shorting is to make the movable electrode bigger, so that the device cannot attain the angle at which the movable electrode touches the fixed one. Subsequently, the maximal tilt angle, denoted by $\theta_{\max}$, is smaller then the touch angle and the system (7) is defined in the restricted state space $\mathcal{X} = \{(\theta, \omega, V_{ap}) \in \mathbb{R}^3 | \theta \in [-\theta_{\max}, \theta_{\max}]\}$.

We make the following basic assumption on the structure of the devices addressed in this study:

Structural Assumption: The structure for positive and negative actuation is identical and the maximal tilt angle is smaller than the one at the position of touch.

For devices whose capacitance is monotonic increasing with respect to θ, γ_θ will be strictly positive and γ'_θ will be non zero and bounded for all $|\theta| \leq \theta_{\max}$, if the above assumption holds.

In order to apply backstepping design, we transform System (7) into the so-called strict-feedback form. Letting $v_{ap} = V_{ap}^2$, denoting

$$\omega_n = \sqrt{\frac{k}{J}}, \xi = \frac{b}{2J\omega_n}, \beta_\theta = \frac{2}{RC_0\left(\rho + \gamma_\theta\right)},$$

and expressing the control signal as the sum of the bias voltage V_B and the actual actuation control u

$$V_{sp} = u + V_B,$$

we obtain

$$\dot{\theta} = \omega \tag{8a}$$

$$\dot{\omega} = \frac{1}{J}\left(-b\omega - k\theta + \frac{C_0}{2}\left(\gamma'_\theta v_{ap} + \gamma'_{-\theta} V_B^2\right)\right) \tag{8b}$$

$$\dot{v}_{ap} = \beta_\theta\left(\sqrt{v_{ap}}(u + V_B) - \left(1 + RC_0\omega\gamma'_\theta\right) v_{ap}\right) \tag{8c}$$

It is important to note that, since $V_{ap} = \pm\sqrt{v_{ap}}$, System (8) represents only one branch of the dynamics of the original system. However, we can see later that it is possible to find a control that will render the domain $\bar{\mathcal{X}} = \{(\theta, \omega, V_{ap}) \in \mathbb{R}^3 | V_{ap} > 0, \theta \in [\theta_{\min}, \theta_{\max}]\}$ invariant. Therefore, no trajectory of the system will cross the boundary $V_{ap} = 0$ and, consequently, (8) is a viable representation of the dynamics of the system. Furthermore, as the electrostatic force is always attractive regardless of the sign of the applied voltage, any feasible operating position can be achieved by using only positive (or negative) actuation voltage.

3. CONTROL SYNTHESIS

We consider in this work the tracking control problem with $y = \theta$ as the output. Following a classical approach, we choose a sufficiently smooth reference trajectory y_d for θ as a function of time and use backstepping to make this trajectory attractive. The design method employed is basically the one introduced by Ngo et al. [2005]. One of the particular feature of their method is that it guarantees the boundness of the virtual control at each step of backstepping, a necessary condition for achieving multiple constraints on state variables. The controller design consists of the following three steps corresponding to the three subsystems expressed in (8).

Step 1: Define the error signal $z_1 = \theta - y_d$. Letting κ_1 be a positive constant representing the desired bound on tracking error z_1, then the desired constraints on the tilt angle can be expressed as

$$\theta_{\min} \leq \underline{y}_d - \kappa_1 \leq \theta \leq \bar{y}_d + \kappa_1 \leq \theta_{\max} \tag{9}$$

where $\underline{y}_d$ and $\bar{y}_d$ are, respectively, the biggest lower bound and the least upper bound of y_d.

A candidate CLF is chosen as

$$V_1 = \frac{k_1}{2}\log\left(\frac{\kappa_1^2}{\kappa_1^2 - z_1^2}\right), \tag{10}$$

where k_1 is a design parameter. As V_1 has a barrier function structure:

$$|z_1| \to \kappa_1 \Rightarrow V_1 \to \infty$$

and the reference trajectory y_d is bounded, z_1 will be bounded by κ_1 if $|z_1(0)| < \kappa_1$ and, consequently, θ will be bounded by (9).

Let α_1 be the virtual control, also called the stabilizing function, and $z_2 = \omega - \alpha_1$ be the corresponding error signal. The time derivative of V_1 along the solutions of the corresponding dynamics is

$$\dot{V}_1 = \frac{k_1 z_1}{\kappa_1^2 - z_1^2}\dot{z}_1 = \frac{k_1 z_1\left(z_2 + \alpha_1 - \dot{y}_d\right)}{\kappa_1^2 - z_1^2}.$$

If the virtual control is chosen as

$$\alpha_1 = -c_1 z_1 + \dot{y}_d, \tag{11}$$

where c_1 is a design parameter, then we have

$$\dot{V}_1 = -\frac{k_1 c_1}{\kappa_1^2 - z_1^2}z_1^2 + \frac{k_1}{\kappa_1^2 - z_1^2}z_1 z_2. \tag{12}$$

Step 2: Similarly to *Step 1*, we augment V_1 by adding another barrier structure:

$$V_2 = V_1 + \frac{k_2}{2}\log\left(\frac{\kappa_2^2}{\kappa_2^2 - z_2^2}\right), \tag{13}$$

where k_2 is a design parameter and κ_2 represents the desired bound on error signal z_2.

The time derivative of V_2 along the solutions of the corresponding dynamics is

$$\begin{aligned}\dot{V}_2 =& \dot{V}_1 + \frac{k_2 z_2}{\kappa_2^2 - z_2^2}\dot{z}_2 \\ =& -\frac{k_1 c_1}{\kappa_1^2 - z_1^2}z_1^2 + \frac{k_1}{\kappa_1^2 - z_1^2}z_1 z_2 + \frac{k_2 z_2}{\kappa_2^2 - z_2^2}\Big(-2\zeta\omega - \omega_n^2\theta \\ &+ \frac{C_0}{J}\left(\gamma'_\theta\left(z_3 + \alpha_2\right) + \gamma'(-\theta)V_B^2 - \dot{\alpha}_1\right)\Big),\end{aligned} \tag{14}$$

where α_2 is the second virtual control and z_3 is the error signal defined as $z_3 = v_{ap} - \alpha_2$. If α_2 is chosen as

$$\alpha_2 = -\frac{\gamma'_{-\theta}}{\gamma'_\theta}V_B^2 + \frac{2J}{C_0\gamma'_\theta}\left(-c_2 z_2 + 2\zeta\omega + \omega_n^2\theta\dot{\alpha}_1\right), \tag{15}$$

where c_2 is a design parameter, then we have

$$\begin{aligned}\dot{V}_2 =& -\frac{k_1 c_1}{\kappa_1^2 - z_1^2}z_1^2 + \frac{k_1}{\kappa_1^2 - z_1^2}z_1 z_2 - \frac{k_2 c_2}{\kappa_2^2 - z_2^2}z_2^2 \\ &+ \frac{\gamma'_\theta C_0}{2J}\frac{k_2}{\kappa_2^2 - z_2^2}z_2 z_3.\end{aligned}$$

Note that in order to keep the virtual control α_2 bounded, one did not try to directly cancel the cross-term $k_1 z_1 z_2 / \left(\kappa_1^2 - z_1^2\right)$ in (14), but rather dominate it by using suitable nonlinear

damping. More specifically, by completing the square, we can express $\dot{V}_2$ as

$$\dot{V}_2 = -W_1 - \frac{k_2 c_2}{2\left(\kappa_2^2 - z_2^2\right)} z_2^2 + \frac{\gamma'_\theta C_0}{2J} \frac{k_2}{\kappa_2^2 - z_2^2} z_2 z_3, \quad (16)$$

where

$$W_1 = \frac{k_1}{2\left(\kappa_1^2 - z_2^2\right)} \left(z_1 - z_2\right)^2 + \frac{k_1 c_1}{\kappa_1^2 - z_1^2} z_1^2 - \frac{k_1}{2\left(\kappa_1^2 - z_1^2\right)} z_1^2 - \frac{k_1}{2\left(\kappa_1^2 - z_1^2\right)} z_2^2 + \frac{k_2 c_2}{2\left(\kappa_2^2 - z_2^2\right)} z_2^2. \quad (17)$$

It has been shown by Ngo et al. [2005] that if

$$c_1 \geq \frac{\kappa_2^2}{\kappa_1^2 \sigma_{z_1}^2} + \frac{1}{2}, \quad (18)$$

where $\sigma_{z_1} \in (0,1)$ is a constant, and

$$c_2 \geq \frac{k_1 \kappa_2^2}{k_2 \kappa_1^2 \left(1 - \sigma_{z_1}^2\right)}, \quad (19)$$

then W_1 is positive-definite in z_1 and z_2.

It can be shown from (15) that α_2 is bounded if the *Structural Assumption* holds and z_2 remains bounded.

Step 3: Finally, in order to bound v_{ap}, it suffices to saturate the error signal z_3. To this end, we augment V_2 by adding a third barrier structure as

$$V = V_2 + \frac{k_3}{2} \log\left(\frac{\kappa_3^2}{\kappa_3^2 - z_3^2}\right), \quad (20)$$

where k_3 is a design parameter and κ_3 is the desired bound on z_3.

The time derivative of V along the solutions of System (8) is given by

$$\begin{aligned}\dot{V} =& \dot{V}_2 + \frac{k_3 z_3}{\kappa_3^2 - z_3^2} \dot{z}_3 \\ =& -W_1(z_1, z_2) - \frac{k_2 c_2}{2\left(\kappa_2^2 - z_2^2\right)} z_2^2 + \frac{\gamma'_\theta C_0}{2J} \frac{k_2}{\kappa_2^2 - z_2^2} z_2 z_3 \\ &+ \frac{k_3}{\kappa_3^2 - z_3^2} z_3 \left(\beta_\theta \left(\sqrt{v_{ap}}(u + V_B) - \left(1 + RC_0 \omega \gamma'_\theta\right) v_{ap}\right) \right. \\ &\left. - \dot{\alpha}_2\right).\end{aligned}$$

We chose a control law of the form

$$u = \frac{1}{\sqrt{v_{ap}}} \left(\frac{\dot{\alpha}_2 - c_3 z_3}{\beta_\theta} - \sqrt{v_{ap}} V_B + \left(1 + RC_0 \omega \gamma'_\theta\right) v_{ap}\right), \quad (21)$$

where c_3 is a design parameter, $\dot{\alpha}_2$ is given by

$$\dot{\alpha}_2 = \left(\frac{\gamma'_{-\theta} \gamma''_\theta}{\gamma'^2_\theta} + \frac{\gamma''_{-\theta}}{\gamma'_\theta}\right) \omega V_B^2 + \frac{2J}{C_0 \gamma'_\theta} \left(-c_2 \dot{z}_2 + 2\zeta \dot{\omega} + \omega_n^2 \omega + \ddot{\alpha}_1\right) - \frac{2J \gamma''_\theta \omega}{C_0 \gamma'^2_\theta} \left(-c_2 z_2 + 2\zeta \omega + \omega_n^2 \theta + \dot{\alpha}_1\right), \quad (22)$$

and $\dot{\alpha}_1$ and $\ddot{\alpha}_1$ can be computed directly from (11). With this control, $\dot{V}$ becomes

$$\dot{V} = -W_1 - W_2, \quad (23)$$

where

$$W_2 = \frac{k_2 c_2}{2\left(\kappa_2^2 - z_2^2\right)} z_2^2 - \frac{\gamma'_\theta C_0}{2J} \frac{k_2}{\kappa_2^2 - z_2^2} z_2 z_3 + \frac{k_3 c_3}{\kappa_3^2 - z_3^2} z_3^2. \quad (24)$$

Similar to the analysis in *Step 2*, we can show that W_2 will be positive-definite if

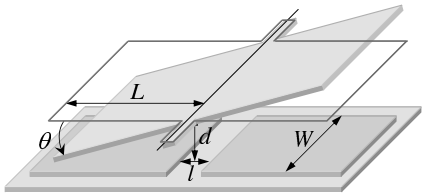

Fig. 4. Schematic representation of the rectangular micro-mirror.

$$c_2 \geq \frac{\kappa_3^2}{\kappa_2^2 \sigma_{z_2}^2} + \frac{1}{2}, \quad (25)$$

where $\sigma_{z_2} \in (0,1)$ is a constant, and

$$c_3 \geq \frac{C_0 \left|\gamma'_\theta\right|_{\max}}{4J} \frac{k_2 \kappa_3^2}{k_3 \kappa_2^2 \left(1 - \sigma_{z_2}^2\right)}. \quad (26)$$

Hence, if the design parameters are tuned in such way that (18), (19), (25), and (26) are all satisfied, then $\dot{V}$ will be negative-definite in the domain

$$\mathcal{D} = \left\{z_i \in \mathbb{R} : |z_i| < \kappa_i, i = 1, 2, 3\right\}. \quad (27)$$

In addition, $V \to \infty$ as $z_i \to \kappa_i$. Therefore $\mathcal{D}$ will be an invariant set and any trajectory starting from the inside of $\mathcal{D}$ will asymptotically converge to the origin. We can thus infer that the closed-loop system is stable.

4. CONTROL OF A RECTANGULAR MICRO-MIRROR

In the following we consider a micro-mirror whose schematic representation is shown in Fig. 4. The geometric, mechanical, and electrical parameters of the device used in the study are those of a micro-mirror in our lab. The values of these parameters are obtained from design specifications and experimental measurements and are given in Table 1.

Table 1. Parameters of the Micro-mirror.

Parameter	Value
Mirror width W	500 (μm)
Mirror length L	230 (μm)
Distance of electrodes l	40 (μm)
Air gap d	12 (μm)
Damping ratio ζ	0.2
Natural frequency ω_n	26500 (rad/s)
Stiffness coefficient k	$3.9\ 10^{-6}$ (N/rad)
Pull-in voltage V_{PIN}	$\sim 280V$
Pull-in angle θ_{PIN}	$\sim 1^\circ$
Maximal tilt angle $\theta_{\max}$	2.7°
Output resistance R	100 (Ω)
Output capacitance C_p	3.0×10^{-7} (F)
Permittivity ε	8.85×10^{-12} (F/m)

As the air gap of this device is much smaller than its extent, the fringing field effect can be ignored (Chan and Dutton [2000]). The capacitance due to a single electrode is then given by

$$C_a = \varepsilon W \int_{\frac{l}{2\cos\theta}}^{L} \frac{dx}{d - x\sin\theta} = \frac{\varepsilon W}{\sin\theta} \ln\left(\frac{d - 0.5l\tan\theta}{d - L\sin\theta}\right), \quad (28)$$

where ε is the permittivity in the air gap, W is the width of the mirror and the electrodes, L is the length of the mirror, l is the distance separating the two electrodes, and d is the air gap. Note that to obtain (28), we suppose that the length of the actuation electrode is sufficiently longer than that of the mirror.

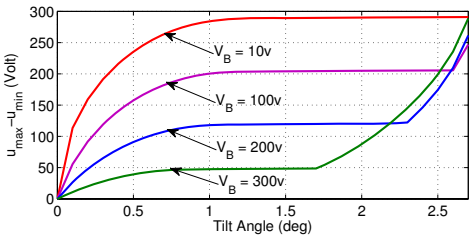

Fig. 5. Dynamical range of the control signal vs. bias voltage.

The capacitance at the flat position is given by

$$C_0 = \frac{\varepsilon W L}{d}, \tag{29}$$

therefore the scaling function can be expressed as

$$\gamma_\theta = \frac{d}{L\sin\theta} \ln\left(\frac{d - 0.5l\tan\theta}{d - L\sin\theta}\right). \tag{30}$$

It is straightforward to verify that the above scaling function satisfies the properties we have imposed earlier in control design.

Note that for a small tilt angle, we have $\sin\theta \approx \theta$. Then the capacitance given in (28) will reduce to a popular formula often used in the literature (see, e.g., Chan and Dutton [2000]) when $l = 0$.

In order to explore the capacity of torque multiplication, a high bias voltage is expected. However, as the actuation voltage curve is highly nonlinear, it is also of interest to minimize the dynamical range of the control signal. A numerical study on the dynamical range of actuation voltage versus different biases has been performed the result of which is shown in Fig. 5. We can see that a bias close to the pull-in voltage can result in an efficient torque multiplication while keeping the dynamical range of the control signal reasonable in a big part of the operating range. It is also preferable to choose a bias lower than the pull-in voltage, in order for the device not to snap down when the control loop is open.

We can follow the line of ideas proposed by Ngo et al. [2005] to find the worst case constraints and to optimize the overall tuning. However, as we deal with a specific device, the controller tuning is based on numerical analysis.

Our objective is to find suitable constraints on tilt angle and actuation voltage, in order to avoid the singularity. We chose then to bound the tilt angle according to $-0.2^\circ \leq \theta \leq 2.7^\circ$. When the bias voltage is fixed to 200 Volts, the corresponding actuation voltage will be bounded as 124.6 Volts $\leq V_{ap} \leq$ 338.6 Volts. The desired bound on angular tracking error is 0.2° and the one on voltage regulation error is 25 Volts. We do not impose an explicit constraint on the angular velocity but only on the corresponding error signal. We choose then $\kappa_1 = 0.0035$, $\kappa_2 = 1$, $\kappa_3 = 25$. For simplicity, we choose $k_1 = k_2 = k_3 = 1$. We obtain $9.5 \leq \gamma'_\theta \leq 318.2$ in the desired operating range. We then tune the controller parameters c_1, c_2, and c_3 by varying the value of α_{z_1} and α_{z_2}.

5. SIMULATION RESULTS

Two reference signals are used in simulations. The first one is a sine wave of the following form:

$$y_d(t) = 0.5A\left(1 + \sin\left(2\pi t/T - \pi/2\right)\right), \tag{31}$$

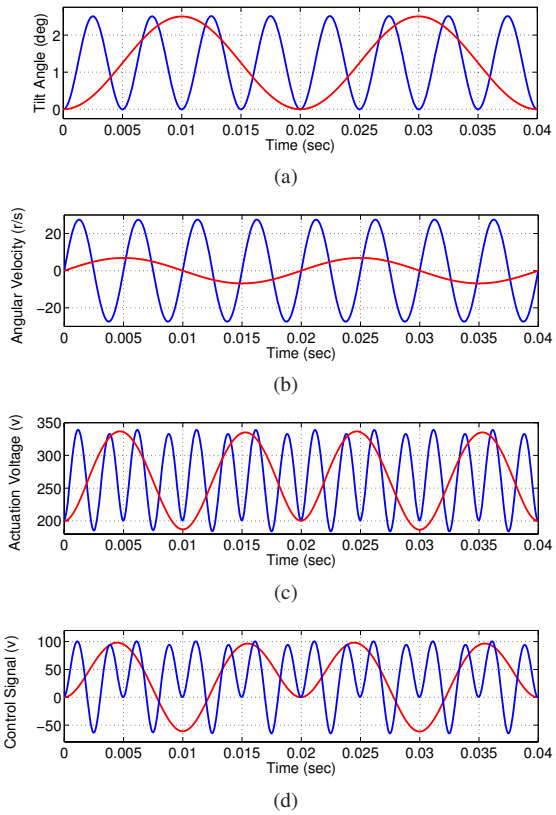

Fig. 6. Closed-loop responses of scanning control: (a) tilt angle θ; (b) angular velocity ω; (c) actuation voltage V_{ap}; (d) control signal u.

where A is the pick-to-pick amplitude and T is the period. This reference trajectory is used for scanning control applications.

Figures 6(a)-6(d) show the simulation results for scanning trajectories with an amplitude of 2.5° and a period of 20ms and 5ms, respectively. It can be seen that the mirror follows smoothly the reference without distortion in the full deflection range while respecting the constraints, hence delivering an enhanced performance. Figure 6(d) shows the control signal u. Obviously, the relationship between the input and the output is highly nonlinear.

The reference trajectory used in set-point control consists of three segments: the initial position, the final position, and a polynomial connecting these two positions, which is of the following form:

$$y_d(t) = \theta(t_i) + (\theta(t_f) - \theta(t_i))\tau^5(t)\sum_{i=0}^{4} a_i\tau^i(t), \tag{32}$$

where $\theta(t_i)$ is the initial tilt angle at time t_i, $\theta(t_f)$ is the desired tilt angle at time t_f, and $\tau(t) \triangleq (t - t_i)/(t_f - t_i)$. The coefficients in (32) can be determined by imposing the initial and final conditions, which yields $a_0 = 126$, $a_1 = -420$, $a_2 = 540$, $a_3 = -315$, and $a_4 = 70$.

Figures 7(a)-7(d) show the simulation results for trajectories bringing the mirror to, respectively, set-point of 2.5° and of 0.5°, and then bring it back to the flat position. The travelling time for each transition is set to 5ms. It can be seen that the controller provides a solid performance and all constraints are respected. It is clear that the system can attain the flat position with a bounded control (see Fig. 7(d)).

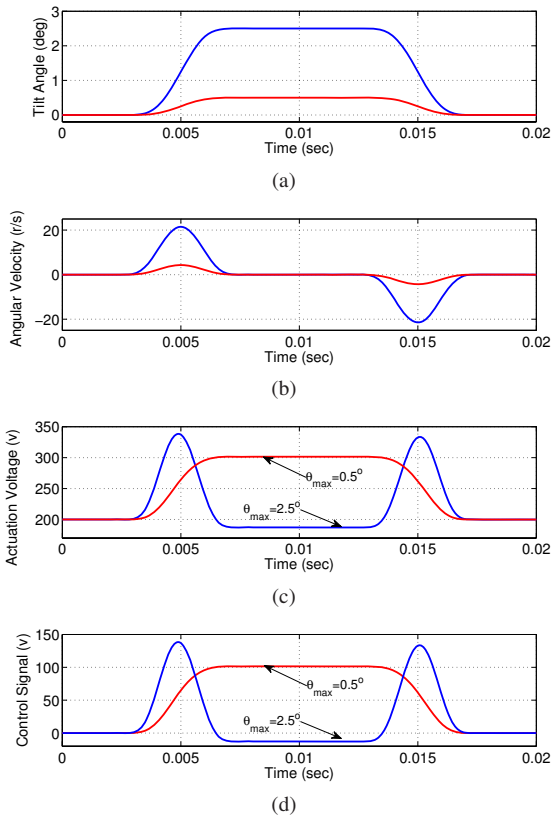

Fig. 7. Closed-loop responses for set-point control: (a) tilt angle θ; (b) angular velocity ω; (c) actuation voltage V_{ap}; (d) control signal u.

Note that for both scanning and set-point control, the maximal amplitude of actuation voltage is considerably reduced compared to the control schemes without bias off-set (see Agudelo et al. [2007a]). This makes the implementation of control systems much easier.

6. CONCLUDING REMARKS

This paper addressed the control of 1DOF torsional micromirrors with constant bias voltage in order to take advantage of torque multiplication and to enhance the controllability at some critical operating points. A generic model of this type of systems, including the electrical subsystems, has been established. A nonlinear control based on backstepping and barrier functions has been developed. It is shown by both stability analysis and numerical simulations that this controller can achieve closed-loop stability in the whole desired operating range while respecting the constraints on state variations and avoiding singularities due to uncontrollability and contact dynamics. Finally, it is worth noting that it is possible to further explore the feature of the structure considered in this work by simultaneously controlling the actuation of the two electrodes as shown in Agudelo et al. [2007b], in order to achieve a two-sided full range actuation.

REFERENCES

C.-G. Agudelo, G. Zhu, M. Packirisamy, and L. Saydy. Flatness-based control of an electrostatic torsional micromirror with voltage feedback. In *Proc. of the IEEE-MWSCAS/NEWCAS'07*, Montreal, Quebec, August 2007a.

C.-G. Agudelo, G. Zhu, and L. Saydy. Nonlinear closed-loop control of an electrostatic torsional micro-mirror by means of differential actuation. In *Proc. of the IEEE-MWSCAS/NEWCAS'07*, Montreal, Quebec, August 2007b.

R. C. Anderson, B. Kawade, D. H. S. Maithripala, K. Ragulan, J. M. Berg, and R. O. Gale. Integrated charge sensors for feedback control of electrostatic MEMS. In *Proc. of the SPIE conference on Smart Structures and Materials 2005*, pages 42–53, San Diego, March 2005.

A. Bemporad. Reference governor for constrained nonlinear systems. *IEEE Trans. Automat. Contr.*, 43(3):415–419, 1998.

A. Bemporad. State and output feedback nonlinear model predictive control: An overview. *European Journal of Control*, 9(2-3):190–207, 2003.

E. K. Chan and R. W. Dutton. Electrostatic micromechanical actuator with extended range of travel. *J. Microelectromech. Syst.*, 9(3):321–328, Spet. 2000.

O. Degani, E. Socher, A. Lipson, T. Leitner, D. J. Setter, S. Kaldor, and Y Nemirovsky. Pull-in study of an electrostatic torsion microactuator. *J. Microelectromech. Syst.*, 7 (4):373–379, 1998.

E. G. Gilbert and I. Kolmanovsky. A generalized reference governor for nonlinear systems. In *Proc. of the 40th IEEE CDC*, pages 4222–4227, Orlando, Florida, December 2001.

L. J. Hornbeck. Deformable-mirror spatial light modulators. In *Spatial Light Modulators and Applications III, SPIE*, volume 1150, pages 86–102, 1990.

D. H. S. Maithripala, J. M. Berg, and W. P. Dayawansa. Control of an electrostatic MEMS using static and dynamic output feedback. *ASME Journal of Dynamic Systems, Measurement and Control*, 127:443–450, 2005.

K. B. Ngo, R. Mahony, and Z. P. Jiang. Integrator backstepping using barrier functions for systems with multiple state constraints. In *Proc. of the 44th IEEE CDC and ECC 2005*, pages 8306–8312, Seville, Spain, December 12-15, 2005.

A. Pareek, M. R. Dokmeci, S. Bakshi, and C. H. Mastrangelo. Torque multiplication and stable range tradeoff in parallel plate angular electrostatic actuators with fixed DC bias. *J. Microelectromech. Syst.*, 14(6):1217–1222, Dec. 2005.

E. Rimon and D. Koditschek. Exact robot navigation using artificial potential functions. *IEEE J. Robot. Automat.*, 8(5): 501–518, 1992.

S. D. Senturia. *Microsystem Design*. Kluwer Academic Publishers, Norwell, MA, 2002.

K. P. Tee, S. Ge, and E. H. Tay. Adaptive control of a class of uncertain electrostatic microactuators. In *Proc. of the 2007 American Control Conference*, pages 3186–3191, New York City, USA, July 11-13, 2006.

J. Wolff and M. Buss. Invariance control design for constrained nonlinear systems. In *Proceedings of the 16th IFAC World Congress*, Prague, Czech Republic, 2005.

G. Zhu, M. Packirisamy, M. Hosseini, and Y.-A. Peter. Modelling and control of an electrostatically actuated torsional micromirror. *Journal of Micromech. Microeng.*, 16(10): 2044–2052, 2006a.

G. Zhu, J. Penet, and L. Saydy. Robust control of an electrostatic actuated MEMS in the presence of parasitics and parameter uncertainties. In *Proc. of the 2006 American Control Conference*, pages 1233–1238, Minneapolis, Minnesota, June 14-16, 2006b.

G. Zhu, J. Lévine, and L. Praly. Stabilization of an electrostatic MEMS including uncontrollable linearization. In *Proc. of the 46th IEEE Conference on Decision and Control*, 2007.